Theor Chem Acc (1999) 102:127–133
DOI 10.1007/s00214980m147

Theoretical
Chemistry Accounts

Regular article

The spin-forbidden reaction $CH(^2\Pi) + N_2 \rightarrow HCN + N(^4S)$ revisited I. Ab initio study of the potential energy surfaces*

Qiang Cui, Keiji Morokuma

Cherry L. Emerson Center for Scientific Computation and Department of Chemistry, Emory University, Atlanta, GA 30322, USA

Received: 23 June 1998 / Accepted: 21 September 1998 / Published online: 8 February 1999

Abstract. High-level ab initio electronic structure theories have been applied to investigate the detailed reaction mechanism of the spin-forbidden reaction $CH(^2\Pi) + N_2 \rightarrow HCN + N(^4S)$. The G2M(RCC) calculations provide accurate energies for the intermediates and transition states involved in the reaction, whereas the B3LYP/6-311G(*d*,*p*) method overestimates the stability of some intermediates by as much as about 10 kcal/mol. A few new structures have been found for both the doublet and quartet electronic states, which are mainly involved in the dative pathways. However, due to the higher energies of these structures, the dominant mechanism remains the one involving the C_{2v} intersystem-crossing step. The C_{2v} minima on the seam of crossing (MSX) structures and the spin-orbit coupling between the doublet and quartet electronic states are rather close to those found in previous studies. Vibrational frequencies orthogonal to the normal of the seam which have been applied in a separate publication to calculate the rate of the $CH(^2\Pi) + N_2 \rightarrow HCN + N(^4S)$ reaction with a newly proposed nonadiabatic transition-state theory for spin-forbidden reactions have been calculated at the MSX from first principles.

Key words: Nonadiabatic processes – Potential energy surfaces

1 Introduction

The reaction $CH(X^2\Pi) + N_2 \rightarrow HCN + N(^4S)$ is of great importance in combustion chemistry, and is believed to be the key step in the production of NO in the reaction zone of hydrocarbon flames [1]. The rate constant measurement of the reaction attracts great attention in the combustion community and has been one of the long-standing issues for the past few decades. The pressure and temperature dependencies of the rate of the reaction indicate that the reaction proceeds via the formation of a long-lived complex, and that different mechanisms dominate at low and high temperatures [2].

It is not surprising that many theoreticians are attracted by the problem. The first detailed work on the reaction mechanism was carried out by Manna and Yarkony [3], who characterized the doublet-quartet crossing structures, and also the spin-orbit coupling elements at the multireference single and double excitation configuration interaction (MRSDCI) level of theory. Two deep minima, a datively bonded structure with short N—N and C—N distances and a C_{2v} structure with a much longer N—N bond, have been found. The low doublet and quartet crossing structure is found in C_{2v}. A linear crossing point was also found, but at a much higher energy. Subsequently, extensive calculations at the level of MRSDCI at the complete active space self-consistent field (CASSCF) optimized geometries were carried out by Martin and Taylor [4], and also by Walch [5]. It is found that a large barrier exists between the dative and the C_{2v} structures, and therefore isomerization between the two does not take place directly. It is also found that no barrier exists between the reactants and the dative minimum, while a barrier of about 0.7 eV is found between the reactants and the C_{2v} minimum. Therefore, the mechanism of the reaction can be summarized as follows

$$\begin{aligned} CH(^2\Pi) + N_2 &\Rightarrow C_{2v}CHN_2(^2A_2) \Rightarrow \text{ Quartet } CHN_2 \\ &\Rightarrow HCN + N(^4S), \\ &\Rightarrow \text{ dative } CHN_2(^2A'') \\ &\Rightarrow \text{ stabilized } CHN_2(^2A'') \ , \end{aligned}$$

and is also depicted in Fig. 1.

The different behavior of the rate constant observed in experiments can therefore be understood by the following. At low temperature, the channel to the dative structure is the only one which is open and the barrierless potential energy surface (PES) results in a negative temperature dependence of the rate constant. At higher temperature, the channel to the C_{2v} structure becomes open, and a normal Arrhenius temperature dependence is expected.

* Contribution to the Kenichi Fukui Memorial Issue

Correspondence to: K. Morokuma

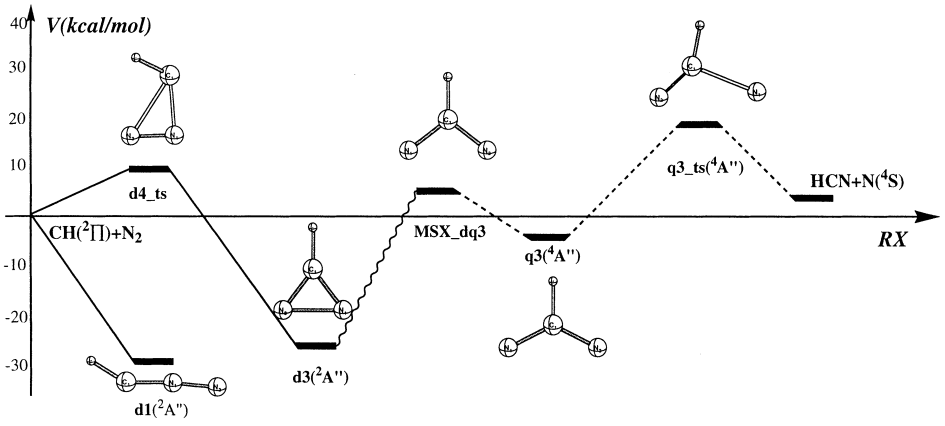

Fig. 1. Simplified schematic potential energy profile for the $CH(^2\Pi) + N_2 \rightarrow HCN + N(^4S)$ reaction proposed by Walch

$$CH\ (^2\Pi) + N_2 \Rightarrow C_{2v}\ CHN_2\ (\mathbf{d3}) \Rightarrow \text{Quartet } CHN_2\ (\mathbf{q3}) \Rightarrow HCN + N(^4S)$$

$$\Rightarrow \text{dative } CHN_2\ (\mathbf{d1}) \Rightarrow \text{stabilized } CHN_2$$

More recently, a 2D model potential surface for the channel involving the C_{2v} pathway was constructed by Seideman and Walch [6]. Furthermore, $N(E)$ and the thermal rate constant for the reaction were calculated using the ABC-DVR technique by Seideman [7] with the model potential. In this study, the reaction was viewed as two unimolecular decay processes coupled by spin-orbit coupling. Furthermore, the cumulative reactive probability was calculated with the Fermi golden rule using the resonance wave function of the doublet and quartet states, and the spin-orbit coupling element from the earlier work of Manaa and Yarkony [3]. To obtain the thermal rate constant, a J-shifting approximation along with the centrifugal sudden approximation has been used. Overall, the reaction probability was found to exhibit a resonance structure which changes from a series of sharp isolated line shapes at low energies to broader overlapping ones at higher energy. The extrapolated thermal rate constant agrees reasonably well with experimental measurements.

Clearly, for all the experimental data as well as for the results from reduced dimensionality quantum mechanical calculations, the current reaction is a perfect system to test the non-adiabatic extension of the transition-state theory (TST) proposed by us recently [8]. However, despite extensive calculations on the electronic structure of the system, there still remain some uncertainties in the barrier heights as well as in the energetics of the crossing point. Some structures found by Martin and Taylor [4] cannot be directly mutually connected, which indicates missing intermediates or transition states. Therefore, we first carried out high-level ab initio calculations to carefully investigate the PESs of the reaction. The data obtained here have been used to calculate the rate constant of the $CH(^2\Pi) + N_2 \rightarrow HCN + N(^4S)$ reaction [8] by combining our nonadiabatic TST with an extended version of Miller's unified statistical theory [9].

2 Computational methods

Structures of the minima, transition states and minima on the seam of crossing (MSX) were first located with the B3LYP [10]/6-311G(*d,p*) [11] method. Intrinsic reaction coordinate [12] calculations were carried out to confirm the two connected structures of each transition state. Some structures of interest including the critical MSX were also optimized at two additional levels: one at the CASSCF [13]/6-311G(*d,p*) level, where a full valence active space excluding the C—H and $2s_N$, namely a (9electron/9orbital) active space was used; the other at the coupled cluster with single and double excitations with triple excitations included as a perturbation CCSD(T) [14]/6-311G(*d,p*) level. Single point energies were also calculated at various correlated levels, including the complete active space second order perturbation (CASPT2) [15]/6-311G(*d,p*), the CCSD(T)/PVTZ [16] and the G2M(RCC) [17] levels. The spin-orbit coupling element around the seam of crossing was calculated with the one-electron Breit–Pauli (BP) Hamiltonian and empirically fit nuclear charges [18] at the CASSCF/6-311G(*d,p*) level.

Density functional theory (DFT) calculations were carried out with the Gaussian94 package [19], and CASSCF/CASPT2 as well as restricted (R)-CCSD(T) calculations were carried out with the Molpro96 program[20]. Unrestricted (U)-CCSD(T) calculations were carried out with ACES-II [21]. In all CCSD(T) calculations the 1*s* core was kept frozen. CASSCF transition-state optimization as well as spin-orbit coupling element calculations were carried out with GAMESS [22]. Optimizations of the MSX were calculated with our own program.

Optimized structures for the doublet and quartet states are shown in Figs. 2 and 3, respectively. The schematic global potential energy profile for the reaction process is shown in Fig. 4. The energies at different levels of theory are listed in Table 1.

3 Results and comparison with previous studies

Since many intermediates of the reaction have already been discussed in previous work, we will not discuss all the structures in detail and shall concentrate on the new structures we have found in the current study. In most of the discussions, only energies at our best-level G2M(RCC) will be referred to.

3.1 The doublet electronic state

First of all, let us discuss the PES of the doublet electronic state. As mentioned in the Introduction, it has been found that two types of CHN_2 complex are produced upon different relative orientation of the reac-

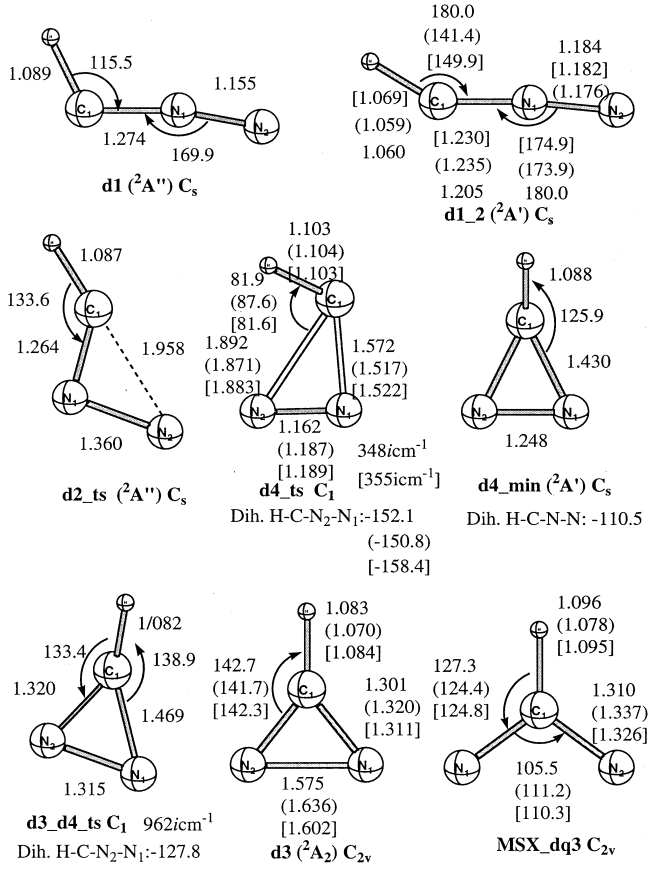

Fig. 2. Optimized structures (in angstroms and degrees) for the intermediates and transition states on the doublet surface. Numbers *without parentheses and brackets*, in *parentheses* and in *brackets* have been calculated at the B3LYP/6-311G(*d,p*), CASSCF/6-311G(*d,p*) and CCSD(T)/6-311G(*d,p*) levels, respectively. For transition states, the imaginary vibrational frequency at the B3LYP/6-311G(*d,p*) level is also given

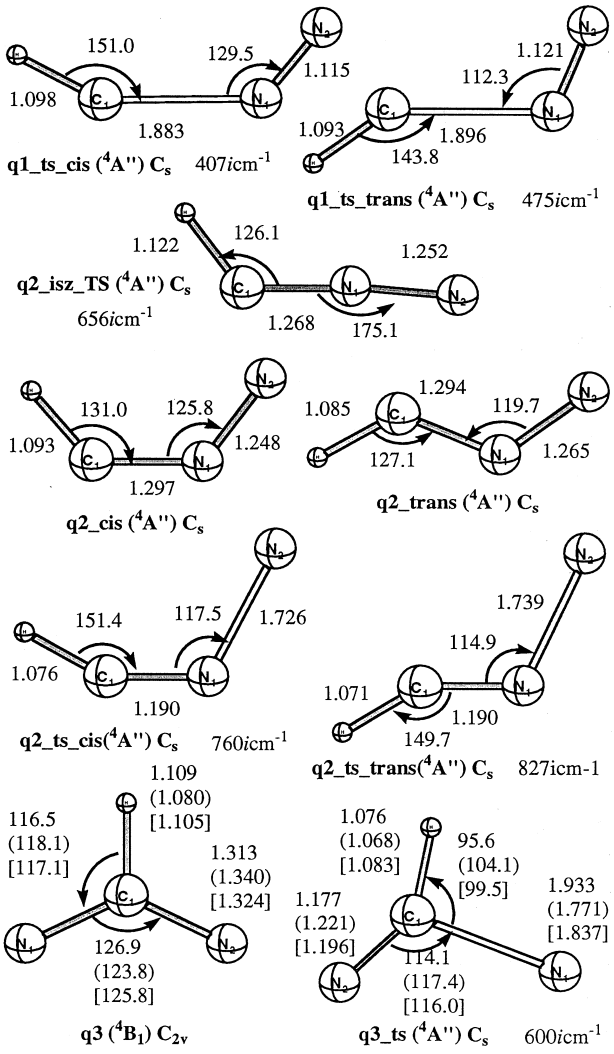

Fig. 3. Optimized structures (in angstroms and degrees) for the intermediates and transition states on the quartet surface. Numbers *without parentheses and brackets*, in *parentheses* and in *brackets* have been calculated at the B3LYP/6-311G(*d,p*), CASSCF/6-311G(*d,p*) and CCSD(T)/6-311G(*d,p*) levels, respectively. For transition states, the imaginary vibrational frequency at the B3LYP/6-311G(*d,p*) level is also given

tants $CH(^2\Pi) + N_2$. One type is the so-called "dative" complex **d1** ($^2A''$) and **d1_2**($^2A'$), where the bonding nature is mainly the strong donation from the N_2 lone-pair to the empty *p* orbital of the $CH(^2\Pi)$. Therefore, the N_2 bond is not much weakened as indicated by the short N—N distance of about 1.16 Å in **d1** and of about 1.18 Å in **d1_2**. In previous calculations, only **d1** ($^2A''$) was considered, and the $^2A'$ state which also correlates to $CH(^2\Pi) + N_2$ was neglected. The optimized structure of the $^2A'$ state is denoted as **d1_2** in Fig. 2. The structure of **d1_2** is quite similar to that of **d1**, except for the H—C—N angle which depends quite sensitively on the level of calculation. As seen in Fig. 2, the value of the H—C—N angle varies from 141.4° at the CASSCF(9/9) level, to 149.9° at the CCSD(T)/6-311G(*d,p*) level, to 180.0° at the B3LYP/6-311G(*d,p*) level. Nevertheless, the potential energy along the H—C—N bending is extremely flat. In Table 1, we have shown both the energies of **d1_2** ($^2A'$) at the CCSD(T)/6-311G(*d,p*) optimized geometry, and those calculated at the linear structure indicated as **d1_2**($^2\Pi$) which was obtained with B3LYP/6-311G(*d,p*). Evidently, the energy difference between the two is very small (~0.2 kcal/mol) at highly correlated levels such as UCCSD(T)/PVTZ and G2M(RCC). The binding energy of CH—N_2 in **d1** is quite large, and depends rather sensitively on the level of calculations as revealed by Table 1. The best estimate at the level of G2M(RCC) is 27.8 kcal/mol with Zero-point energy (ZPE) correction. The B3LYP/6-311G(*d,p*) method overestimates the binding energy rather significantly by about 10 kcal/mol. The binding energy of CH—N_2 is smaller in **d1_2**($^2A'$) than in **d1** ($^2A''$) by about 11 kcal/mol at the G2M(RCC) level, and this can be rationalized by noting the following two factors. First of all, significant sp^2 hybridization has occurred in **d1**, but not in **d1_2**, as manifested by the H—C—N angle of about 116° in **d1** and of about 180° in **d1_2**. Secondly, the N—N π bond is weakened to a larger extent in **d1_2** than in **d1**, as manifested by the longer N—N distance in **d1_2**, which might come from the repulsion from the π

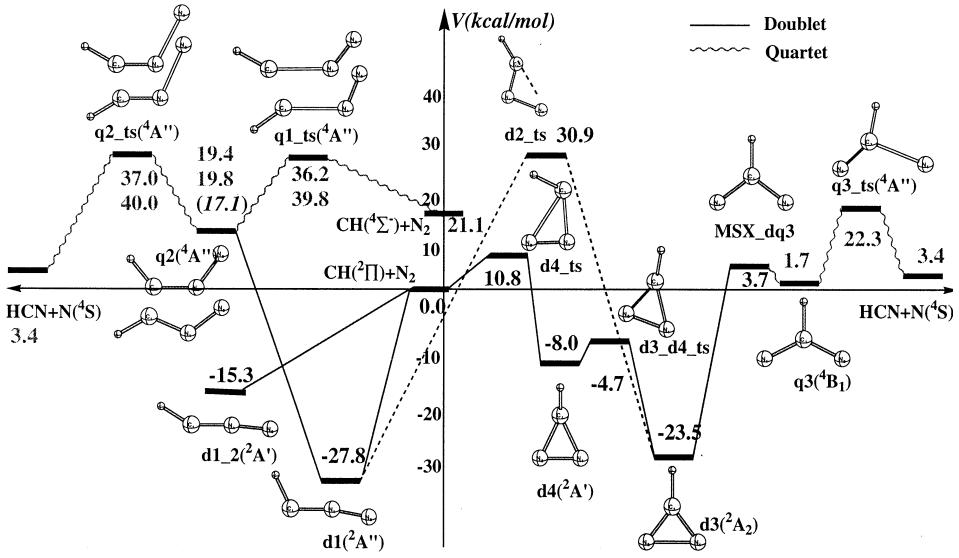

Fig. 4. Global potential energy profile, obtained in the present work, for the reaction of $CH(^2\Pi) + N_2 \rightarrow HCN + N(^4S)$. The relative energies are calculated with G2M(RCC), including B3LYP/6-311G(*d*,*p*) zero-point energy

electrons on $CH(^2A')$. The two factors work in the same direction and make **d1** ($^2A''$) more stable. Finally, it should be noted that no encounter barrier has been found for either **d1** or **d1_2** from the reactants, which is probably what one expects for dative complexes.

The path leading to the other type of CHN_2 complex, the so-called C_{2v} complex **d3** ($^2A_2$) has been explored by Walch [6] and will not be discussed in detail here. Briefly, $CH(^2\Pi)$ and N_2 first form a C_s complex **d4** ($^2A'$) through the C_1 transition state **d4_ts**. The barrier height is calculated to be 10.8 kcal/mol at the G2M(RCC) level with ZPE correction. In **d4**, the C—N bonds are single bonds in character as indicated by the length of 1.430 Å, and the N—N bond is still a double bond as indicated by the length of 1.248 Å. The C atom is already sp^3 hybridized which is manifested by the nonplanar structure of **d4**. The CH—N_2 binding energy of **d4** is calculated to be 8.0 kcal/mol at the G2M(RCC) level including ZPE correction. After overcoming a small barrier at the structure **d3_d4_ts**, a stable C_{2v} complex **d3** ($^2A_2$) is formed. In **d3**, the C—N bonds are double bonds in character, and N—N is a single bond, as revealed by their lengths of about 1.30 and about 1.60 Å, respectively. The energy of **d3** relative to the reactants also depends quite significantly on the level of calculation; it is 23.5 kcal/mol at the G2M(RCC) level with ZPE correction. It should be noted that other electronic states of **d3** are much higher in energy, because excitation of electrons into π^* or σ^* orbitals has to be involved.

Martin and Tayor [4] were the first to point out that a large barrier has to be overcome for the isomerization between **d1** and **d3**. This is also verified by our calculation, where the transition state **d2_ts** ($^2A''$) has been found to lie 27.1 kcal/mol above the reactants at the G2M(RCC) level with ZPE correction. In other words, the isomerization barrier is 50.6 kcal/mol measured from **d3**. Consequently, the dative complex and the C_{2v} complex channels can be considered separately for most thermal conditions. Since the other electronic states of **d3** are high in energy, we did not look for the isomerization barrier from the **d1_2** structure.

3.2 The quartet electronic state

Let us now move to the quartet electronic state. Similarly to the doublet state, the quartet state PES can also be characterized by two pathways: the dative path and the C_{2v} path. The C_{2v} path includes the well-characterized C_{2v} minimum **q3**($^4B_1$) and the subsequent dissociation transition state **q3_ts** ($^4A''$) shown in Fig. 3. They can be accessed at relatively low energy only through the intersystem crossing from the C_{2v} region on the doublet-state surface. The **q3** and **q3_ts** are calculated to be 2.0 kcal/mol lower and 22.3 kcal/mol higher than the doublet reactants, respectively, at the G2M(RCC) level with ZPE correction.

The dative path on the quartet electronic state surface has not been clearly characterized before, and in fact some structures found by Martin and Taylor [4] were not identified correctly. According to our calculations, HCN + N(^4S) can be formed directly from the quartet reactants of $CH(^4\Sigma^-) + N_2$ via the two energetically similar dative pathways where HCNN adopts cis or trans conformations. We have located two encounter transition states **q1_ts_cis**, and **q1_ts_trans**, in which the C—N distances are rather long (~1.9 Å), as shown in Fig. 3. The energies calculated at the G2M(RCC) level with ZPE correction are 36.2 kcal/mol and 39.8 kcal/mol above the doublet reactants for **q1_ts_cis** and **q1_ts_trans**, respectively. The two transition states lead to cis and trans dative minima, **q2_cis** and **q2_trans**, respectively. The N—N π bonds are weakened significantly compared to the doublet dative structure **d1**, as indicated by the longer N—N distance in **q2_cis** and **q2_trans**, which obviously comes from the excitation of an electron to the π^*_{N-N} orbital in the quartet state. The energies measured from the doublet reactants were calculated at the G2M(RCC) level with ZPE correction to be 19.4 and 19.8 kcal/mol for the cis and trans minima,

Table 1. Energies of critical structures in the reaction of CH + N_2[a]

Method Basis[b]	B3LYP I	PMP4 I	PMP4 II	PMP4 III	RCCSD(T) I	MP 2 I	MP 2 II	MP 2 III	MP 2 IV	G2M(RCC)[c]	UCCSD(T) V	CASPTZ I	ZPE[d] I
$CH(^2\Pi) + N_2$	0.0	0.0	0.0	0.0	0.0	0.0	0.0	0.0	0.0	0.0	0.0	0.0	7.5
$CH(^4\Sigma^-) + N_2$	20.3	12.3	12.8	14.6	13.4	6.6	7.1	8.9	9.6	19.8	15.7		7.8
$HCN + N(^4S)$	−1.7	−7.7	−6.6	−5.2	−6.9	−10.2	−9.2	−7.7	−6.2	0.6	−3.5	−6.8	10.3
d1($^2A''$)	−42.5	−26.5	−25.9	−32.3	−25.9	−14.7	−14.1	−20.9	−21.1	−32.0	−30.1	−22.1	11.7
d1_2($^2A'$)	−30.9	−13.6	−13.3	−19.7	−11.8	−2.1	−1.7	−8.1	−8.6	−18.6	−16.9		
d1_2′($^2\Pi$)	−31.6	−14.5	−14.3	−21.3	−11.0	−8.2	−8.0	−14.9	−15.6	−18.4	−16.8	−8.5	10.6
d2_ts($^2A''$)	23.3	43.7	42.9	40.2	33.4	54.3	53.8	51.7	50.9	29.0	29.9		9.4
d3($^2A_2$)	−32.6	−23.2	−24.5	−29.4	−22.2	−17.0	−17.3	−22.3	−23.3	−28.2	−25.6	−21.5	12.2
d4($^2A'$)	−15.9	−9.1	−8.6	−12.5	−8.0	−12.7	−12.2	−16.5	−17.6	−12.6	−10.6	−7.6	12.1
d3_d4_ts(^2A)	−13.2	−3.6	−3.4	−7.5	−2.9	6.8	7.1	2.7	1.4	−8.1	−5.9	−2.0	10.9
d4_ts(^2A)	4.8	10.7	11.2	7.3	12.2	14.2	14.8	10.4	10.2	8.5	11.8	14.2	9.8
q1_ts_cis($^4A''$)	25.5	30.7	31.1	30.9	29.8	33.8	34.3	33.7	34.5	34.5	30.0		9.2
q1_ts_tran($^4A''$)	27.6	33.2	35.5	33.3	32.0	37.7	38.2	37.6	38.5	38.5	32.0		8.8
q2_cis($^4A''$)	−0.4	17.0	16.9	15.0	14.8	25.2	25.3	23.4	23.0	15.7	12.6	18.3	11.2
q2_tran($^4A''$)	0.1	16.7	16.2	15.1	15.0	25.1	24.7	23.6	22.9	16.0	12.6	15.3	11.3
q2_tran($^2A''$)	−0.3	19.4	19.1	16.8	17.0	30.1	29.8	27.9	27.2	17.1	14.2	20.8	
q2_isz_ts($^4A''$)	25.9	46.0	46.0	42.9	44.4	53.3	53.4	50.5	50.2	44.4	41.4		9.7
q2_ts_cis($^4A''$)	21.6	33.1	33.2	32.6	31.0	44.4	44.6	43.9	44.5	34.5	30.4		10.0
q2_ts_tran($^4A''$)	24.6	36.8	36.6	36.4	34.4	48.3	48.2	47.9	48.3	37.7	33.7		9.8
q3($^4B_1$)	−17.3	−3.4	−3.7	−4.4	−4.0	8.0	7.8	7.4	7.2	−1.9	−5.6	−3.7	11.1
MSX_dq3($^2A''$)	−4.3	2.5	2.0	1.7	1.0	13.8	13.5	13.4	13.0	3.0	0.3	1.9	11.1
MSX_dq3($^4A''$)	−4.3	−3.1	−4.3	−6.0	1.9	14.3	13.3	11.3	10.2	−2.2	−0.4	−0.2	10.4
q3_ts($^4A''$)	10.2	17.0	17.1	17.6	14.6	28.0	28.1	28.6	29.5	19.5	15.5	15.9	10.3

[a] Energies (kcal/mol) without zero-point energy. For CASPT2 calculations, the CASSCF/6-311G(*d*,*p*) optimized geometries have been used. For all others except for **d1_2** (see text), the B3LYP/6-311G(*d*, *p*) geometries have been used

[b] Basis notations are: I: 6-311G(*d*,*p*), II: 6-311 + G(*d*,*p*), III: 6-311G(2*df*,*p*), IV: 6-311 + G(3*df*,2*p*), V: PVTZ

[c] No zero-point energy included even in the G2M energies, to be consistent with the rest of the table

[d] At the B3LYP/6-311G(*d*,*p*) level

[e] The energy of the $^2A''$ state at the $^4A''$ geometry

respectively. An isomerization TS, **q2_isz_TS**, was found between **q2_cis** and **q2_trans**, and the isomerization barrier measured from **q2_cis** is 25.2 kcal/mol at the G2M(RCC) level with ZPE correction.

Two dissociation transition states with cis and trans conformations were also found (**q2_ts_cis** and **q2_ts_trans** in Fig. 3). The characters of the two transition states are obvious from the long N—N distance (~1.7 Å). At the level of G2M(RCC) with ZPE correction, the two transition states with cis and trans conformations lie at 37.0 and 40.0 kcal/mol, respectively. Compared to the quartet dissociation transition state **q3_ts** in the C_{2v} path, the dissociation transition states in the dative channel are much higher in energy. In addition, the encounter transition states **q1_ts_cis** and **q1_ts_trans** are also high in energy; therefore the dative path for the quartet state is not expected to compete with the intersystem-crossing mechanism at low energy. At high energy, however, the dative channel might compete effectively provided that $CH(^4\Sigma^-)$ is populated. The energy of entire reaction of $CH(^2\Pi) + N_2 \rightarrow HCN + N(^4S)$ is calculated to be 3.4 kcal/mol at the G2M(RCC) level of theory with ZPE correction.

3.3 The crossing structures between doublet and quartet states

In the well-established intersystem-crossing mechanism for the reaction, the doublet and the quartet electronic states form a seam surface around the C_{2v} region between **d3** and **q3**. In the current study, we restricted ourselves to a C_{2v} search since the distortion was insignificant. The optimized MSX between doublet ($^2A_2$) and quartet ($^4B_1$) at different levels is shown in Fig. 2 as **MSX_dq3**, and is very close to the C_{2v} structure of Manaa and Yarkony [3]. As can be seen clearly, the motion that brings doublet and quartet together is nearly exclusively that of the N—C—N angle or the N—N distance, while other degrees of freedom do not change significantly. This is not very surprising since the change in the electronic structure from **d3** to **q3** is mainly the $\sigma_{N-N} \rightarrow \sigma^*_{N-N}$ excitation. It should be noted that the contribution of the triples (T) is significant in the CCSD calculations for the seam of crossing. At the UCCSD(T)/6-311G(*d*,*p*) optimized MSX, the doublet and the quartet are separated by about 6.0 kcal/mol at the CCSD/6-311G(*d*,*p*) or the CCSD/PVTZ level without triples correction. The effect of the basis set is small, as the singlet-triplet separation is 0.7 kcal/mol at the UCCSD(T)/PVTZ level at the UCCSD(T)/6-311G(*d*,*p*) optimized MSX. At the G2M(RCC) level without ZPE, the doublet-quartet averaged energy of the **MSX_dq3** lies at nearly the same energy as the doublet reactants. The spin-orbit coupling element at the level of CASSCF(9,9)/6-311G(*d*,*p*) at **MSX_dq3** is calculated to be 8.0 cm^{-1}, in reasonable agreement with the 11.1 cm^{-1} of Manaa and Yarkony [3] with the full BP Hamiltonian [23]/spin-orbit CI approach.

We also tried to locate MSX between the doublet and the quartet for the dative channel. The search for MSX between $^2A''$ and $^4A''$ at the B3LYP/6-311G(*d*,*p*) level ended up with a structure very close to the trans minimum on the quartet-state surface, **q2_trans**. Indeed, as shown in Table 1, the energy of the $^2A''$ state is very close to that of the $^4A''$ state at the **q2_trans** geometry. The spin-orbit coupling element is calculated to be 5.1 cm^{-1}. Judging from the higher energy of **q2_trans**, and the smaller spin-orbit coupling element between $^2A''$ and $^4A''$ compared to those of **MSX_dq3**, the dative intersystem-crossing channel is not expected to be able to compete with the C_{2v} intersystem-crossing mechanism. In addition, the higher exit barrier in the dative channel, **q2_ts_cis/trans**, compared to that in the C_{2v} channel **q3_ts**, also suggests that the C_{2v} intersystem crossing will be the dominant pathway for the entire reaction. For the same reason, we did not look for additional MSX between the $^2A'$ and $^4A''$ states, although a larger spin-orbit coupling element might be expected.

Putting all the findings together, the overall potential energy profiles for the spin-forbidden reaction $CH(^2\Pi) + N_2 \rightarrow HCN + N(^4S)$ are shown in Fig. 4. Although a few new structures have been found, the relative energies indicate that the dominant mechanism for the entire reaction remains unchanged from the one proposed by Walch; namely, starting from the reactants, the formation of the C_{2v} complex **d3** via the **d4_ts** transition state, followed by intersystem crossing at **MSX_dq3** from the doublet to the quartet to reach a Y-shaped quartet intermediate **q3**, and its subsequent dissociation via **q3_ts** to give the final products.

A straightforward extension of TST to nonadiabatic reactions was proposed by us recently [8]. The detailed description of the theory and application to the current reaction will be published seperately, and here we will concentrate on one essential piece of information required in the rate constant calculations: the vibrational frequencies orthogonal to the normal of the seam at the MSX. As described in Ref. [8] the algorithm for such a calculation is very similar to that of generalized normal mode analysis commonly used in the minimum-energy-path-based variational TST calculations. The 3*N*-7 frequencies obtained at the MSX are shown in Table 2, along with vibrational frequencies for other important complexes involved in the C_{2v} intersystem-crossing pathway. The vibrational frequencies at the MSX for the doublet and the quartet states differ by some amount, up to as much as 20%. It was suspected in the beginning that this difference comes from the convergence criteria of the MSX. In a recent publication [24] Baboul and Schlegel discussed the importance of convergence criteria of both the transition state and the reaction path in projected frequency calculations. A not tightly converged reaction path may cause a numerical error as large as 1400 cm^{-1} in the C—H vibrational frequency. We have therefore recalculated the vibrational frequencies at the MSX optimized with very tight criteria. At this structure, the energy difference between the doublet and the quartet electronic states is 6.6×10^{-4} cm^{-1}, and the projected force of the two electronic states on the seam is smaller than 5.6×10^{-7} hartree/bohr. The projected vibrational frequencies calculated at this structure are within 1 cm^{-1} of those shown in Table 2, which were

Table 2. Vibrational frequencies for the critical structures involved in the C_{2v} intersystem-crossing pathway for the reaction of CH + N_2

Structure	Frequencies[a] (cm^{-1})
$CH(^2\Pi)$, N_2	2804.3, 2447.0
d3($^2A_2$)	718.1, 838.7, 926.3, 1193.3, 1636.4, 3206.2
	650.5, 857.6, 925.6, 1212.0, 1610.2, 3256.0
d4_ts(^2A)	347.8i, 300.9, 600.4, 1036.2, 1900.7, 3008.2
	355i, 271.3, 654.2, 973.0, 1763.3, 3073.9
MSX_dq3($^2A_2$)	943.2, 948.3, 1370.7, 1476.0, 3025.8
MSX_dq3($^4B_1$)	797.4, 1005.0, 1059.7, 1358.6, 3040.8
	785.2, 965.8, 1101.1, 1298.9, 3079.8
q3($^4B_1$)	562.0, 809.1, 1103.4, 1187.4, 1225.2, 2886.5
	551.2, 804.5, 1038.1, 1190.6, 1216.9, 2986.1
q3_ts($^4A''$)	599.7i, 349.2, 741.1, 866.2, 1929.5, 3294.6
	799.3i, 375.2, 718.7, 910.3, 1823.9, 3267.3

[a] The numbers in plain text are obtained at the B3LYP/6-311G (*d*, *p*) level at the structures optimized at the same level, and the numbers in italics are calculated with the UCCSD(T)/6-311G(*d*, *p*) method at the corresponding optimized structures

calculated at the MSX structure optimized with the standard convergence criteria (projected force on the seam $< 5 \times 10^{-4}$ hartree/bohr, $\Delta E \sim 4$ cm^{-1}). Therefore, the difference in the projected vibrational frequencies of the two electronic states seems to come from the definition of the normal of the seam, which is expressed as the gradient of the energy difference. As a result, there are some errors in the degeneracy condition starting from the second order. It should also be noted that the B3LYP/6-311G(*d*,*p*) frequencies are in most cases very close to the CCSD(T)/6-311G(*d*,*p*) ones, including at the MSX structures. It has recently been pointed out that one should be cautious of the performance of DFT when different spin states are close in energy, since DFT only gives the projected spin quantum number M rather than the S^2 value [25]. Although we agree with such statements in general, our results indicate that B3LYP behaves rather well for the present system.

4 Conclusions

The detailed reaction mechanism of the spin-forbidden reaction $CH(^2\Pi) + N_2 \rightarrow HCN + N(^4S)$ has been studied carefully with high-level ab initio electronic structure theories. G2M(RCC) calculations provide accurate energies for the intermediates and transition states involved in the reaction. Compared to G2M(RCC), B3LYP with a triple zeta plus polarization basis set overestimates the stabilities of some intermediates by as much as about 10 kcal/mol. A few new structures have been found for both the doublet and quartet electronic states, which are mainly involved in the dative pathways. However, due to the higher energies of these structures, the dominant mechanism remains the C_{2v} intersystem-crossing mechanism summarized by Walch [5]. The C_{2v} MSX structures and the spin-orbit coupling between the doublet and quartet electronic states are rather close to those found in previous studies. Vibrational frequencies orthogonal to the normal of the seam have been calculated at the MSX, and the numerical values for the low vibrational modes are found not to be sensitive to the convergence criteria for the MSX optimization. The vibrational frequencies and the energies from this study have been applied to calculate the rate of the $CH(^2\Pi) + N_2 \rightarrow HCN + N(^4S)$ reaction with a newly proposed nonadiabatic TST for spin-forbidden reactions [8].

Acknowledgements. Q.C acknowledges a graduate fellowship from the Phillips Petroleum Co. The use of computational facilities and software at the Emerson Center is acknowledged. This work was in part supported by grants F49620-95-1-0182 and F49620-98-1-0063 from the Air Force Office of Scientific Research. Dedicated to Prof. Kenichi Fukui, who taught me science and beyond.

References

1. Miller JA, Bowman CT (1989) Prog Energy Combust Sci 15: 287
2. Bozzelli JW, Karim MHU, Dean AM (1993) Proceedings of the 6th Toyota Conference on Turbulence and Molecular Processes in Combustion. Elsevier, New York
3. (a) Manaa MR, Yarkony DR (1991) J Chem Phys 95: 1808; (b) Manaa MR, Yarkony DR (1991) Chem Phys Lett 188: 352
4. Martin JML, Taylor PR (1993) Chem Phys Lett 209: 143
5. Walch SP (1993) Chem Phys Lett 208: 214
6. Seideman T, Walch SP (1994) J Chem Phys 101: 3656
7. Seideman T (1994) J Chem Phys 101: 3662
8. Cui Q, Morokuma K, Bowman JM, Klippenstein SJ J Chem Phys (submitted)
9. Miller WH (1976) J Chem Phys 65: 2216
10. (a) Becke AD (1988) Phys Rev A 38: 3098; (b) Lee C, Yang W, Parr RG (1988) Phys Rev B 37: 785; (c) Becke AD (1993) J Chem Phys 98: 5648
11. Krishnan R, Binkley JS, Seeger R, Pople JA (1980) J Chem Phys 72: 650
12. (a) Fukui K (1981) Acc Chem Res 14: 363; (b) Kato S, Morokuma K (1980) J Chem Phys 73: 3900
13. Werner H-J (1987) Adv Chem Phys 79: 1
14. Bartlett RJ (1995) In: Yarkony DR (ed) Modern electronic structure theory. World Scientific, Singapore
15. Anderson K, Roos B (1995) In: Yarkony DR (ed) Modern electronic structure theory. World Scientific, Singapore
16. (a) Dunning TH Jr (1989) J Chem Phys 90: 1007; (b) Kendall RA, Dunning TH Jr, Harrison RJ (1992) J Chem Phys 96: 6796
17. Mebel AM, Morokuma K, Lin MC (1995) J Chem Phys 103: 7414
18. Koseki S, Schimidt MW, Gordon MS (1992) J Phys Chem 96: 10768
19. Frisch MJ, Trucks GW, Schlegel HB, Gill PMW, Johnson BG, Robb MA, Cheeseman JR, Keith T, Petersson GA, Montgomery JA, Raghavachari K, Al-Laham MA, Zakrzewski VG, Ortiz JV, Foresman JB, Peng CY, Ayala PY, Chen W, Wong MW, Andres JL, Replogle ES, Gomperts R, Martin RL, Fox DJ, Binkley JS, Defrees DJ, Baker J, Stewart JP, Head-Gordon M, Gonzalez C, Pople JA (1995) Gaussian, Gaussian 94, revision D.3. Pittsburg
20. Knowles PJ, Werner H-J, Molpro96.4. University of Birmingham, Birmingham, UK
21. Stanton JF, Gauss J, Lauderdale WJ, Watts JD, Bartlett RJ ACES-II. Florida State University
22. Schmidt MW, Baldridge KK, Boatz JA, Elbert ST, Gordon MS, Jensen JH, Koseki S, Matsunaga N, Nguyen KA, Su SJ, Windus TL, Dupuis M, Montgomery JS (1993) J Comput Chem 14: 1347
23. (a) Havriliak SJ, Yarkony DR (1985) J Chem Phys 83: 1168; (b) Yarkony DR (1986) J Chem Phys 84: 2075
24. Baboul AB, Schlegel HB (1997) J Chem Phys 107: 9413
25. Davidson ER (1998) J Comput Chem 69: 241